Helmholtz-Zentrum Geesthacht
Zentrum für Material- und Küstenforschung

Final Draft
of the original manuscript:

Lebedev, V.; Kulvelis, Y.; Voronin, A.; Komolkin, A.; Kyzyma, E.; Tropin, T.; Garamus, V.:
Mechanisms of supramolecular ordering of water-soluble derivatives of fullerenes in aqueous media.
In: Fullerenes, Nanotubes and Carbon Nanostructures. Vol. 28 (2020) 1, 30 - 39.
First published online by Taylor & Francis: 29.09.2019

DOI: 10.1080/1536383X.2019.1671362
https://dx.doi.org/10.1080/1536383X.2019.1671362

Mechanisms of supramolecular ordering of watersoluble derivatives of fullerenes in aqueous media

V. T. Lebedev1, Yu. V. Kulvelis1, A. S. Voronin2, A. V. Komolkin2, E. A. Kyzyma3,4, T. V. Tropin3 & V. M. Garamus5

[1]*B.P.Konstantinov Petersburg Nuclear Physics Institute, NRC Kurchatov Institute,Gatchina, Russia*
[2]*Saint Petersburg State University, Saint Petersburg, Russia*
[3]*Joint Institute for Nuclear Research, Dubna, Russia*
[4]*Taras Shevchenko National University of Kyiv, Kyiv, Ukraine*
[5]*Helmholtz-Zentrum Geesthacht:Centre for Materials and Coastal Research, Geesthacht, Germany*

Fullerenols C60(OH)X and C70(OH)X (X _ 30) have been studied in aqueous solutions at the concentrations 0.05–22wt% by X-ray and neutron scattering and using modeling hydroxyls' arrangements on carbon cages to explain the molecular assembly defined by hydrophobic and hydrophilic interactions of molecules. In the case of C60 quantum chemical calculations minimizing molecular energy for different configurations of OH-groups on the carbon cages showed their preferred localization at C60 spheroids' equatorial zone and at the opposite poles. However, less symmetric hydroxyls' localization on C70 molecules was found since hydroxyls do not create closed chains on them. As a result, the molecules C60(OH)X are associated into primary chain-like aggregates (_20 units, few nanometers in size) more likely in water than the fullerenols C70(OH)X forming similar groups of lower aggregation degree. For C60(OH)X and C70(OH)X the peculiarities in hydroxyls' grafting affected a coordination of primary groups integrated into secondary and tertiary structures at the distances R _ 5 nm and R _ 30nm at the concentrations C>5wt% and C>10wt%, respectively. The discovered mechanism of fullerenols' assembly in water will facilitate their use in chemistry and biomedicine.

1. Introduction

Much research of physico-chemical and biological properties of fullerene C_{60} water-soluble derivatives was carried out during last decades. The studies of antioxidant and neuroprotective properties [1–3], photodynamic activity [4], cytotoxicity [5,6] should be mentioned in this respect. In certain *in vitro* and *in vivo* experiments it was established that in biological systems a hydroxylated derivative, $C_{60}(OH)_{24}$ (fullerenol), may serve as an effective antioxidant agent and free radical acceptor [7]. Fullerenols also possess protective properties both against toxic chemicals (pesticides) [8] and in the case of radiation-induced toxicity [9].

In fact, the implementation of fullerenes' water-soluble derivatives in medical practices is nearly impossible without a fundamental understanding of their behavior in different media, and, primarily, in water. To date, organic solutions and aqueous dispersions of C_{60} and C_{70} are the most studied systems due to their availability and relative simplicity of preparation [10–12]. A characteristic feature of such systems is clusters formation and growth. The sizes of clusters are in the range of 1-1000 nm, measured using light, X-rays and neutrons scattering, optical absorption [13–16] and other methods. In turn, functionalized fullerenes in aqueous media containing biological molecules form large clusters also due to binding with DNA, surfactants and lipids [17]. Thereby, types and numbers of functional groups have a significant impact on fullerenes and endofullerenes' derivatives behavior in solutions and their tendencies to aggregation [18].

Meanwhile, experimental and theoretical studies of hydroxylated fullerenes are often non-systematic and not detailed. A few quantitative parameters, such as aggregation number and its correlation with composition or pH factor, are usually reported. The problem of consistent study of structure and behavior of fullerenes' derivatives in aqueous media still remains very important. Moreover, this study may produce some advancement in biomedical applications. The present work is devoted to the investigation of the structure and interaction mechanisms of hydroxylated chromatographically pure fullerenes C_{60} and C_{70} in aqueous solutions by small-angle neutron, X-ray and dynamic light scattering in connection with subtle features of these entities' chemical structure evaluated by quantum chemical modeling.

2. Materials and methods

Hydroxylated derivatives of fullerenes, $C_{60}(OH)_{30}$ and $C_{70}(OH)_{30}$ fullerenols, were synthesized by the method [19] developed at the Laboratory of Neutron Physicochemical Researches (NRC «Kurchatov Institute» – PNPI). The synthesis included two-phase reaction in aqueous solution of ammonia, C_{60} and C_{70} in ortho-xylene with a TBAH interfacial catalyst (tetrabutylammonium hydroxide). The chemical purity of the initial fullerenes C_{60} ($\geq$ 99.5%) and C_{70} ($\geq$ 99.5%) was estimated by the means of the Shimadzu LC-20 chromatograph. At the first stage of synthesis fullerenols with a low degree of hydroxylation were obtained. Further, at the second stage, they were additionally treated using hydrogen peroxide to produce highly hydroxylated fullerenols. Detailed information about the synthesis of fullerenols can be found in Suppl. 1.

Fullerenols hydroxylation was confirmed via IR-spectroscopy. The FTIR-spectra have been measured on powder samples in the KBr matrix using the Fourier-transform IR-spectrometer FSM 12-01 (FTIR). The spectra of the initial C_{60} (C_{70}) fullerenes have characteristic peaks at 527, 576, 1182, 1428 cm^{-1} (533, 641, 672, 1086, 1132, 1427 cm^{-1}). After hydroxylation additional peaks at 1081, 1387, 1626, 1721 cm^{-1} and 1063, 1380, 1642, 1721, 3423 cm^{-1} have appeared in the FTIR-spectra of the hydroxylated fullerenes C_{60} and C_{70}, respectively. The bands at 3423 cm^{-1} and 1385 cm^{-1} are characteristic for νO-H and δO-H oscillations. The band at 1620 cm^{-1} corresponds to νC=O bonding

vibrations, and the band at 1078 cm^{-1} - for νC-O oscillations. The number of hydroxyl groups was estimated by measuring thermal elimination of substituents [20]. The results allowed to identify the samples as highly hydroxylated substances $C_{60}(OH)_x$ and $C_{70}(OH)_x$ with $x = 30 \pm 2$.

Calculations of the structures and energies of various isomers of $C_{60}(OH)_{2,4,6,20,30}$ and $C_{70}(OH)_{30}$ fullerenols have been carried out using Gaussian-16 software [21] in the Resource Park of the St. Petersburg State University "Computing Center of St. Petersburg State University". After constructing the initial configuration of each isomer in the Jmol program [22], the geometry of isomer was optimized by the Hartree-Fock RHF method with the 6-31G basis set [23]. For accounting the correlation energy the B3LYP functional [24,25] was added. After these two steps, the isomers with the lowest energy (not exceeding the minimum energy of 0.1 Hartree or 250 kJ/mol) were selected. Finally, a calculation was performed for them at the level of B3LYP/6-31G++(d). The error in the energy value for all isomers in their optimal geometry was of $1 \cdot 10^{-3}$ kJ/mol.

During computing the account of a certain number of local energy minima for each isomer there has to be taken care of. To do this, the orientation of the OH-groups must be considered. If for the given isomer all OH-groups form hydrogen bonds, and no pairs of oxygen atoms with overlapping electron densities (electronic sp^3-clouds) exist, then the configuration most probably corresponds to the absolute energy minimum. Therefore, when constructing the initial geometry, all OH-groups were oriented this way. Link?

The structural state of fullerenols $C_{60}(OH)_{30}$ and $C_{70}(OH)_{30}$ in aqueous solutions of different concentrations where studied by small-angle neutron and X-Rays scattering (SANS, SAXS) and dynamic-light scattering (DLS) methods. The solutions were prepared by adding fullerene component to the water, its content was restricted by the limits of solubility, 15.3 % for $C_{60}(OH)_{30}$ and 22.4 % for $C_{70}(OH)_{30}$. With concentration growth, the pH of solutions has decreased to a constant value of ~2.5, that indicated a dissociation of OH-groups on fullerenes: Ful(OH)x⇆Ful(O)-x + H+ (Fig.S1).

Self-assembly of fullerenols in aqueous solutions (concentrations C = 0.8-8 % wt.) and gel-like systems (C = 10-22% wt.) has been studied by SANS, carried out on the “Membrana-2” diffractometer~~,~~ at Petersburg Nuclear Physics Institute, NRC Kurchatov Institute. The range of momentum transfer (scattering vector) $q = (4\pi/\lambda)\sin(\theta/2)$ was 0.04 – 0.8 nm^{-1} (θ - the scattering angle, λ = 0.3 nm - the wavelength, $\Delta\lambda/\lambda = 0.25$ - the spectral width). The neutron scattering intensities curves were measured for the 1 mm thick samples, and corrected for the background (solvent) and direct (not scattered) beam. The data were further normalized to the transmissions of the samples for neutrons (~70 %). The transmissions for the aqueous buffer and the samples have differed not more than 1% even for high concentrations. This pointed to a predominantly single scattering on fullerenols in solutions. Beam attenuation in the sample was primarily determined by incoherent scattering on protons in water and in hydroxyls of fullerenols. ~~Normalizing the intensities on the similar values found for the standard (1-mm-thick layer of H_2O), we evaluated the scattering cross-sections of the samples in absolute units (cm^{-1}) per 1 cm^3 of volume in unit solid angle (Ω). A contribution of aqueous buffer was subtracted from the resulting values. Finally, we analyzed the momentum transfer dependencies of the coherent cross-sections $d\Sigma(q)/d\Omega$.~~

The low concentrated fullerenols solutions (C = 0.05 - 1 % wt.) were measured by SAXS at the P12 BioSAXS Beamline at PETRA III ring, EMBL/DESY using the 100 (V) μm × 200 (H) μm X-ray beam, energy 10 keV. The sample-to-detector distance, 3.1 m, provided the q-range of 0.07-4.6 nm^{-1} calibrated with silver behenate [26]. Scattering patterns were registered by the Pilatus 2M pixel detector. The solutions (approximately 20 μL) were injected into the sample capillary using an automated liquid handling sample changer. In order to reduce the risk of radiation damage, the samples were moved slightly during the exposure. Twenty consecutive frames (each 0.05 s) comprising the measurement of the sample and buffer were performed. To check if artifacts have occurred as a result

of radiation damage, all scattering curves of a recorded dataset were compared to a reference measurement (typically the first exposure) and verified data were finally integrated by automated acquisition program [27]. Before and after each SAXS measurement of the sample, a signal from pure buffer was measured and used for background subtraction. The data were normalized to transmitted beam.

The SANS and SAXS data processing has been carried out using the ATSAS software package [28]. Further, the earlier developed approach [29] was used to visualize in detail the structural features of aggregates in solutions.

The monotonously decreasing scattering, obtained in the experiments, can be generally described by the following model function:

$$d\Sigma / d\Omega(q) = \frac{I_0}{(1 + (R_C q)^2)^{D/2}} + B \qquad (1)$$

The forward cross-section $I_0 = I_{q\to 0}$ results from the data extrapolation in the limit q→0. The observed structures with a correlation radius R_C are described by ~~epy~~ squared form-factor $F^2(q) = 1/[1 + (R_C q)^2]^{D/2}$ having an asymptotic form $\sim 1/q^D$ at $q >> 1/R_C$. The exponent D characterizes molecular packing in the structures of size $\sim R_C$ (fractal clusters). The parameter B represents an incoherent background mainly due to the scattering on protons.

The respective correlation functions $\gamma(R)$, and the normalized pair-distribution functions, $P_N(R)=P(R)/C=\gamma(R)R^2/C$, were obtained and analyzed using ATSAS software. The fitting of the corresponding functions requires three exponentials for both neutron and X-rays scattering experiments. At higher concentrations (C ≥ 1.9 % wt., SANS data), the following expression was used for the $\gamma(R)$ function:

$$\gamma(R) = g_1 e^{-R/R_1} + g_2 e^{-R/R_2} + g_3 e^{-(R-L)^2/R_3^2} \qquad (2)$$

The model function (2) consists of a contributions of small molecular groups (correlation radius R_1, first term), which form larger structures (radius R_2, second term) coordinated at characteristic distance L with dispersion R_3 (third term).

Fit of the experimental data using Eq. (2) gives the amplitudes g_i, radii R_i (i=1,2,3) and further the corresponding aggregation and coordination numbers, m_i. For both fullerenols, the aggregation numbers m_1 were calculated using partial scattering cross-sections of the solutions:

$$\sigma_{01} = m_1 \left(\Delta K_F\right)^2 \varphi v_F \qquad (3)$$

in the q→0 limit. The parameter ΔK_F in (3) is the contrast factor of fullerenol molecule (with the volume v_F) relative to the solvent, φ is the volume fraction of fullerenols in solution. The value $\sigma_{01} = 4\pi\int \gamma_1(R)R^2 dR$ is the integral of the respective correlation function, $\gamma_1(R) = g_1\exp(-R/R_1)$. Similar integrals σ_{02} and σ_{03} were found using the functions $\gamma_2(R)$ and $\gamma_3(R)$ being the second and the third terms in (2). The values of m_2 and m_3 are calculated as $m_2=\sigma_{02}/\sigma_{01}$ and $m_3=\sigma_{03}/\sigma_{01}$.

For lower concentrations, (C ≤ 1 % wt., SAXS data) the fitting of $P_N(R)$ was performed using the following expression:

$$P_N(R) = g_1 R^2 e^{-R/R_{C1}} + g_2 R^2 e^{-(R-L_A)^2/R_{C2}^2} + g_3 R^2 e^{-R/R_{C3}} \qquad (4)$$

In (4), the components with the amplitudes g_1, g_2, g_3 describe various molecular correlations at different scales (R_{C1}, L_A, R_{C2}, R_{C3}). The first term characterizes primary objects (molecules, tiny groups) having inner correlation radius R_{C1}. At very low concentrations (C = 0.05; 0.1%) the second term (positive amplitude g_2, parameter $L_A = 0$) serves to model an attraction between a primary object and similar surrounding units at the radii $R \leq R_{C2}$. Along with it, the third term (positive amplitude g_3) describes more extended association trends of primary objects at $R \leq R_{C3}$.

Связь между R_i и R_{Ci}??? Связь между L и L_A?! Почему в (2) – второе слагаемое особого вида, а в (3) – третье?! Формула (2) – для описания C=0.05-1.0%, формула (3) – для C>1.9%! Нужно еще раз сюда вернуться и поработать! Какой смысл, если это разные диапазоны, использовать разные функции – только путаем всё.

DLS has been performed on $C_{70}(OH)_{30}$ fullerenols diluted systems (C = 0.1 wt. %) on the original spectrometer (PNPI, NRC Kurchatov Institute). The laser wavelength was 633 nm. Different scattering angles of 20°, 30°, 45°, 60° in low-frequency (1, 2, and 4 kHz) and high-frequency (16, 32 and 64 kHz) spectral bands were used in order to detect large aggregates and also to resolve the fine fractions [30,31]. The spectrum analyzer was IBM compatible multifunction ADC/DAC module on USB1.1 bus with ADSP2185M signal processor ("Analog Devices, Inc"), developed by ZAO "L-CARD" (Russia). Data processing based on the regularization method [31,32] allowed restoring the distributions of hydrodynamic radii of different fractions of particles in solutions.

3. Results

DFT calculations. Analysis shows that in case of two OH-groups' addition to C_{60} the most probable structure is OH connection to C-atoms pairing two hexagons. The groups' addition to remote or bound carbon atoms along the conjugation of 6- and 5-membered rings turns out to be less probable. Further, we considered increase of OH-groups number from two to four, and further up to six. In this case, the most favorable is the formation of the elongated chain of OH-groups along the double bonds. The chain is not closed around one C_6 ring and all hydrogen atoms have to form hydrogen bonds with the neighboring oxygen atom. In C_{60} fullerene, the longest chain satisfying these requirements has a length of 20 atoms located along the molecule's "equator" (Fig. 1a). A similar structure was obtained and described in Ref. [33]. The isomer $C_{60}(OH)_{30}$ with the lowest energy also has this 20-atoms chain. Three additional chains are present, two of which are composed of four OH-groups and are localized at the "poles", and another one is composed of two OH-groups (Fig. 1b).

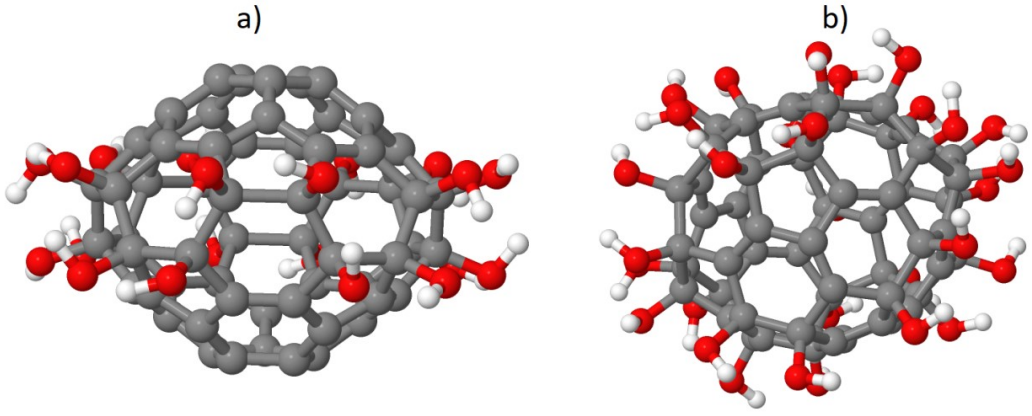

Fig. 1. Schematic presentation of fullerenol isomers (obtained by DFT method): a) $C_{60}(OH)_{20}$ isomer; b) $C_{60}(OH)_{30}$ isomer. Grey spheres – C atoms, red – O, white – H.

In C_{70} molecule some double bonds are located along the conjugation of the C_6 and C_5 rings (Fig. 2b). In $C_{70}(OH)_n$, the disjoint chain situated along the double bonds consists of 26 OH-groups and is not closed. To construct $C_{70}(OH)_{30}$ it is necessary to add the second chain of four hydroxyls (Fig. 2, isomer 1). This isomer has the lowest energy among all the six calculated models. Fig. 2 also shows two additional isomers (2, 3), with closest energies to the first one.

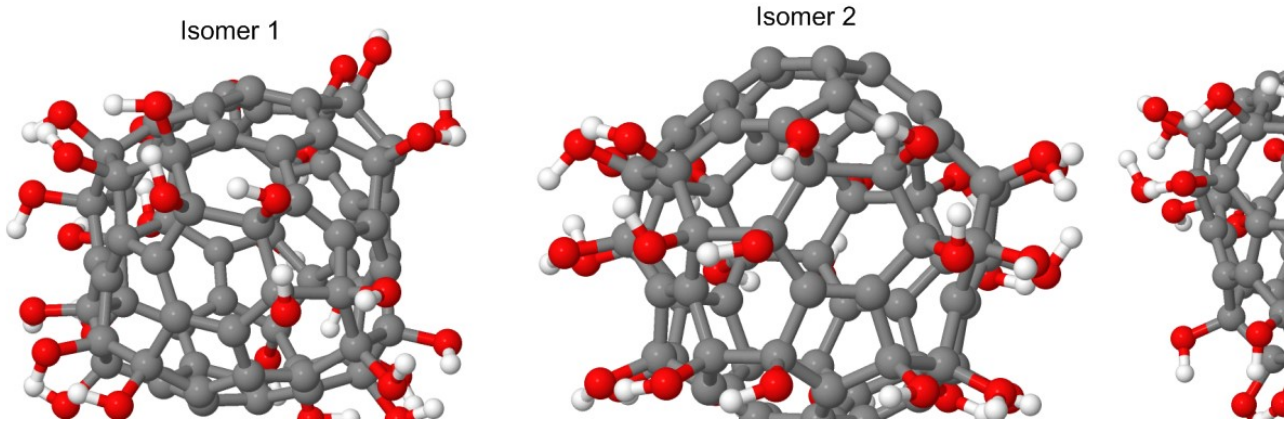

Fig. 2. Isomers of the $C_{70}(OH)_{30}$ molecule with the lowest relative energies, obtained by the DFT method.

Not uniform distribution of hydroxyls on the cages of C_{60} and C_{70} results in the presence of hydrophobic and hydrophilic areas and obviously may have a significant effect on the behavior of fullerenols in aqueous medium. The molecular stacking via hydrophobic fragments on fullerenols' surface and the formation of various supramolecular structures (chain-like, branched globular) in solutions is possible. The SANS, SAXS and DLS experiments were performed to recognize the mechanisms of $C_{60}(OH)_{30}$ and $C_{70}(OH)_{30}$ self-assembly.

SANS measurements. SANS spectra of $C_{60}(OH)_{30}$ and $C_{70}(OH)_{30}$ solutions are presented on Fig. 3 (a, b). The cross sections decrease proving existence of molecular correlations at the distances $R \sim 2\pi/q \geq 10^1$ nm greatly exceeding the fullerenols size ~1.3 nm. Moreover, the data (Fig.3) roughly obey the power-law, $d\Sigma(q)/d\Omega \sim q^D$, where the exponent D of power-law, characterizing the molecular packing of clusters, is in the $D = 1\text{-}5/3$ (а в русском тексте – 5/3-2!) interval, that corresponds to scattering on rod-like particles (D~1) or Flory exponent for statistically coiled chains with excluded volume (D~5/3).

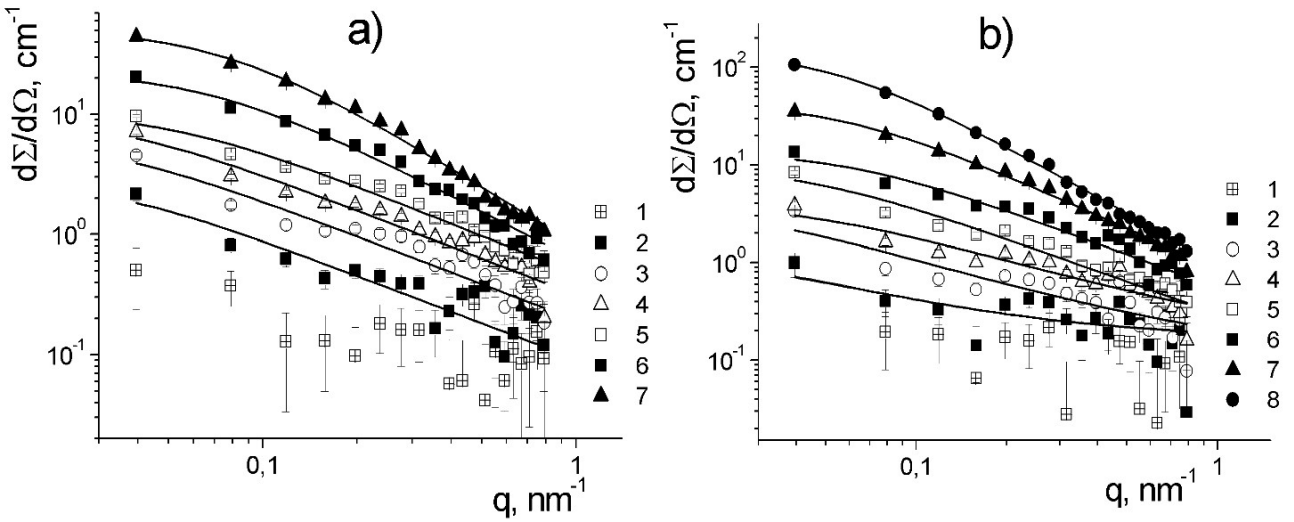

Fig. 3. The scattering cross sections *vs*. momentum transfer q for the solutions of fullerenols $C_{60}(OH)_{30}$ (a) and $C_{70}(OH)_{30}$ (b) at the concentrations C = 0.8; 1.9; 3.5; 5.2; 7.2; 10.5; 15.3; 22.4 wt. %. (1-8). Lines present respective fits using Eq. (1). Нужно раскрасить?! В русской версии – цветные рисунки!

The scattering curves in Fig. 3 for $C_{60}(OH)_{30}$ are relatively higher than those for similar concentrations of $C_{70}(OH)_{30}$. This is an indication of a stronger aggregation of $C_{60}(OH)_{30}$. Qualitatively the behavior of cross sections is similar for both fullerenols and does not undergo any crucial changes when their concentration in solution is increased. Thus, a relative stability of fullerenols assemblies is observed. The growth of forward cross section with increase of concentration denotes the formation of larger amounts of aggregates. At the same time, the index D increases from 1 to 1.7 reflecting the altering from straightened to curved chains, while their correlation radii R_C decrease: for $C_{60}(OH)_{30}$ from 33 to 13 nm and for $C_{70}(OH)_{30}$ - from 37 to 17 nm, i.e. the structures become more compact. Где эти данные по зависимости от конценрации?! Я бы вообще графики построил!

A more detailed analysis of the structural features of fullerenols at different concentrations in solutions was performed for the normalized pair-distribution functions $P_N(R)$ (Figs. 4,5). The peak observed in the interval $R = 0 – 5$ nm indicates the coordination of molecules with the nearest environment. This primary structural level is characterized by small formations with the sizes below 5 nm. The further decrease (and even negative values) of $P_N(R)$ in the ~10-25 nm range characterizes repulsion between these compact aggregates. ~~Such small particles interact to each other weakly due to the repulsive forces.~~ Outside this repulsion region (R>20-25 nm), the particles are distributed at characteristic distances $R \sim 30$ nm corresponding to the maximum of the peak in $P_N(R)$.

For the lowest concentration (C = 1.9 wt. %) the spectra are plotted separately (Fig. 4) to display a discrete nature of correlations particularly manifested in the dilute systems.

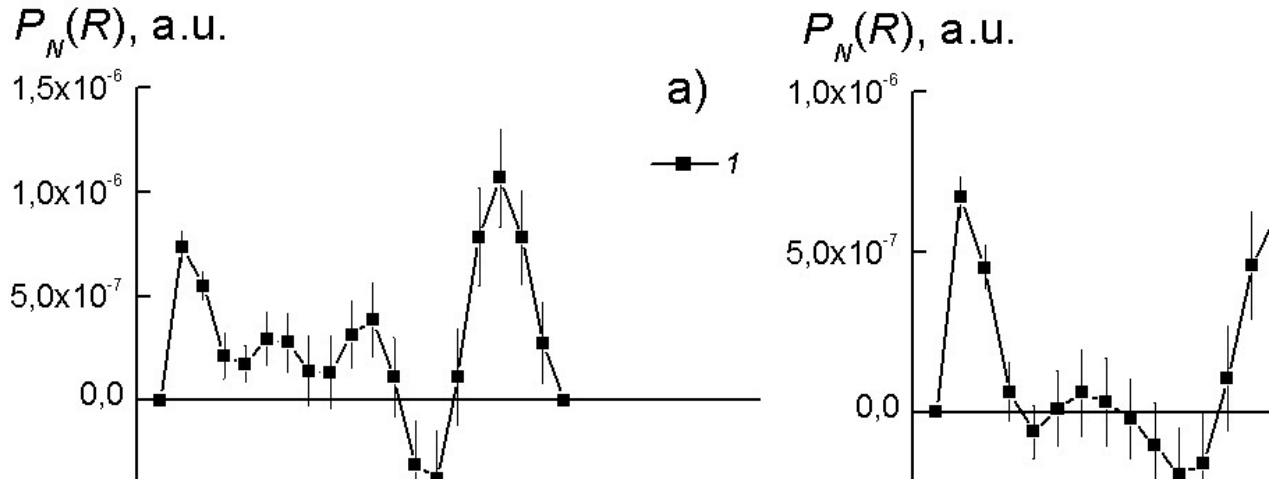

Fig. 4. Normalized pair-distribution functions $P_N(R)$ for the $C_{60}(OH)_{30}$ (a) and $C_{70}(OH)_{30}$ (b) aqueous solutions at the concentration C = 1.9 % wt. (1).

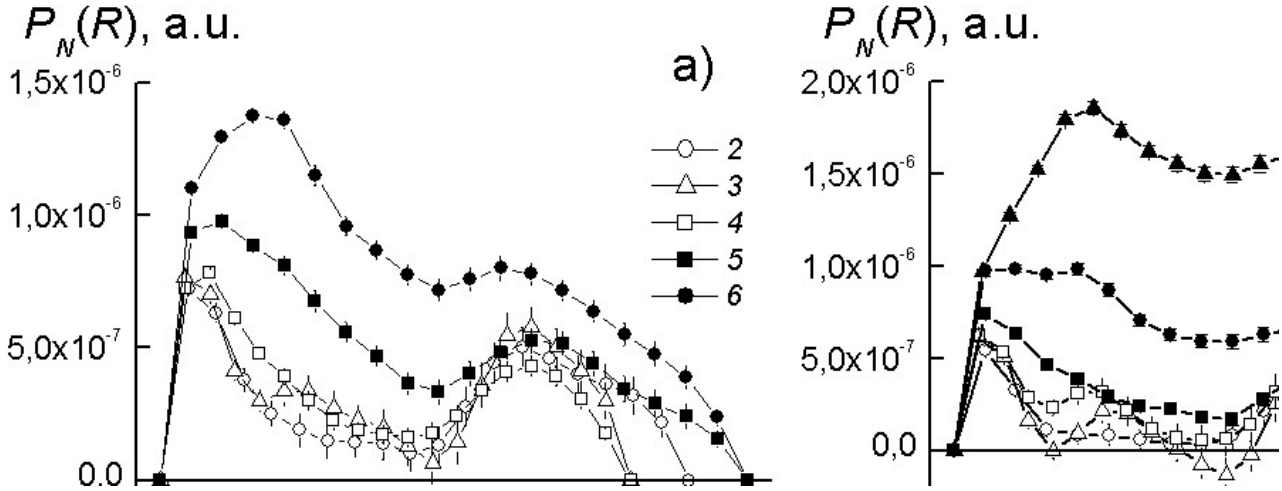

Fig. 5. Normalized pair-distribution functions $P_N(R)$ for the $C_{60}(OH)_{30}$ (a) and $C_{70}(OH)_{30}$ (b) aqueous solutions at different concentrations C = 3.5; 5.2; 7.2; 10.5; 15.3; 22.4 (2-7) wt. %.

SAXS measurements. At the lowest concentration the spectral features for both systems with $C_{60}(OH)_{30}$ and $C_{70}(OH)_{30}$ are quite similar. However, the excluded volume effects are more pronounced for $C_{70}(OH)_{30}$. The increasing of fullerenols' concentrations up to ~7 wt. % (for $C_{60}(OH)_{30}$) and to ~10 wt. % (for $C_{70}(OH)_{30}$) does not qualitatively change the $P_N(R)$ spectra (Fig.5). Thus, as the concentration of solution increases, the new structures similar to the existing ones are formed. The overlapping and compaction of structures is noticeable at the concentrations ~ 10-15 wt. % for $C_{60}(OH)_{30}$ and 10-20 wt. % for $C_{70}(OH)_{30}$, as follows from the broadening and shifting of characteristic $P_N(R)$ peaks, and increasing of their amplitudes (Fig. 5 a, b).

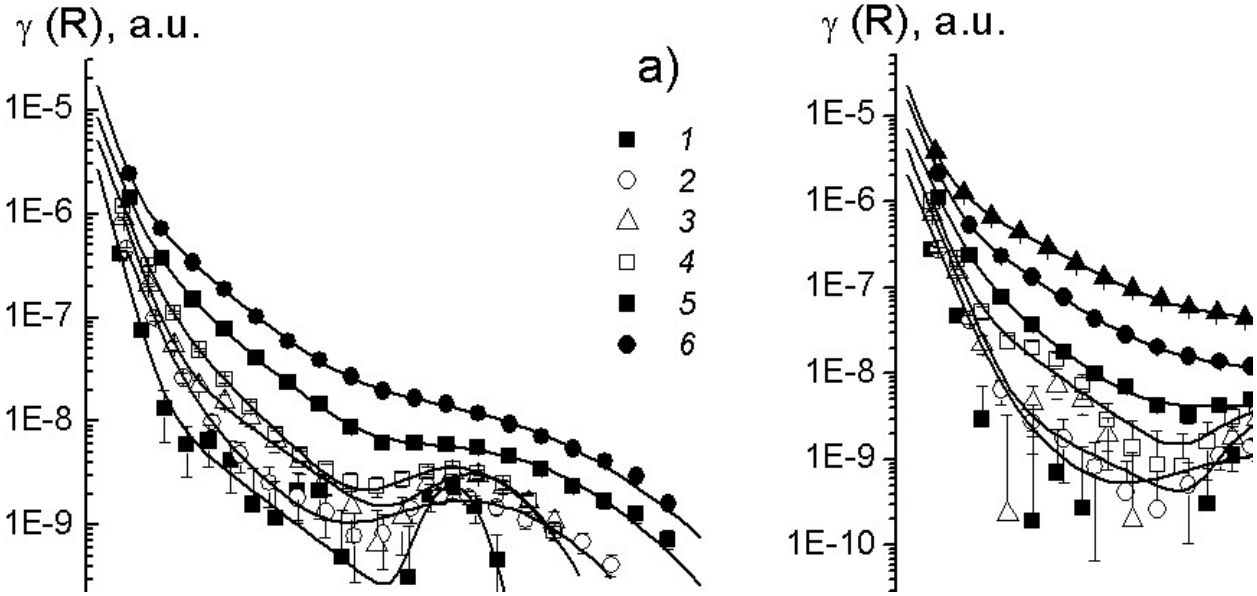

Fig.6. Correlation functions $\gamma(R)$ for aqueous solutions of fullerenols $C_{60}(OH)_{30}$ (a) and $C_{70}(OH)_{30}$ (b). Concentrations: C = 1.9; 3.5; 5.2; 7.2; 10.5; 15.3; 22.4 wt. %. (1-7). Curves are fitting functions,Eq. (2).

The parameters of fullerenols structural organization were obtained through the approximation of the correlation functions $\gamma(R)$ via Eq. (2). The aggregation numbers of particles, m_i, for the clusters of each structural level were obtained using Eq. (3). This analysis allowed describing the ordering of $C_{60}(OH)_{30}$ and $C_{70}(OH)_{30}$ in solutions, where the macromolecules become stronger correlated at different structural levels (scales R_1, R_2, L) as the concentration increases, C = 2 → 20 wt. %. We obtain, that both fullerenols in solutions at the concentrations C = 2-20 wt. % are grouped within the first sphere (radius R_1 ~ 1.0-1.4 nm), where m_1 ~ 10-20 molecules are localized (Fig.S2). In turn, such a primary group is coordinated with m_2 ~ 1-10 neighboring groups within the sphere, characterized by the correlation radius R_2 ~ 4-7 nm. The gyration radius of these regions of correlations is $R_{G2} = 6^{1/2} \cdot R_2$ ~ 10-17 nm. Thus diameter ~ $2R_{G2}$ ~ 20-30 nm defines the spacing between the groups, L ~ 30 nm, in the case of contacts. Hence, the environment of a secondary unit is detected at distances R ~ L ~ 30 nm where similar aggregates are localized. They total number of coordinated primary (or secondary?) groups is m_3 ~ 2-8. For both fullerenols, the degree of association in primary groups, m_1 ~ 10-20, remains nearly constant, but the integration strengthens at the second and the third structural levels, thus the corresponding coordination numbers increase by one order in magnitude as the concentration increases (Fig.S2).

Certain differences in fullerenols behavior were observed. In $C_{60}(OH)_{30}$ solutions of low or moderate content (C ≤ 5 wt.%) a primary group is coordinated barely with m_2 ~ 1-2 groups. But at higher concentrations (C > 5 wt.%) the integration becomes stronger at the second and third levels, m_2 ~ m_3 ~ 10 (R ~ 5-30 nm). In the case of $C_{70}(OH)_{30}$, the local molecular ordering is somewhat different. At C ≤ 10 wt.% the primary groups do not trend to join, m_2 ~ 0.2-0.3, at the scale R ~ 4-7 nm. Although repulsive forces between primary groups dominate at short radii, at larger distances R ~ L ~ 30 nm molecular attraction is stronger and stimulates gathering, m_3 ~ 2-3. At higher $C_{70}(OH)_{30}$ concentrations, C > 10 wt. %, the aggregation is strengthened at the second level, m_2 ~ 5-10 (similar to $C_{60}(OH)_{30}$ solutions), as well as at the third structural level but less intensively, m_3/m_2 ~ 0.5. Thus, in highly concentrated systems of $C_{70}(OH)_{30}$ and $C_{60}(OH)_{30}$ the assembly is similar.

The SAXS experiments were aimed at evaluating the limits of multilevel structuring in diluted systems. In synchrotron experiments several low concentrated aqueous solutions (light water) of $C_{70}(OH)_{30}$ (C = 0.05 -1.0 wt. %) were examined.

At low concentrations a qualitative change in scattering patterns was observed (Fig. 7a). In very diluted systems (C = 0.05 - 0.1 wt. %) the intensity increases and reaches a plateau at 0.1 $nm^{-1} \leq q \leq 0.5$ nm^{-1}. This is an indication of some molecular assemblies (~10 nm) in solutions. Moreover, at lower $q \leq$ 0.1 nm^{-1} further intensity increase testifies an association of these structures into larger formations ~ 10^1 nm. At a certain concentration, C* = 0.2 wt. %, the scattering pattern is qualitatively different (Fig. 7a, data 3). The q-dependence of cross sections is non-monotonous. The observed intensity decrease at lower edge of the q-range is characteristic for dense systems of particles with mutual repulsion. Это не глюк? In other words, some excluded volume effects are revealed at a critical concentration, C = C*. Further enrichment of the system, C> C*, reinforces a long-range aggregation inducing intense scattering at lower edge of the q-range (Fig.7a, data 4, 5).

The structural peculiarities are more evident in the $P(R)$ function obtained from the SAXS data (Fig. 7b, Fig. S3). In the concentration range C=0.05-1.0 wt.% the $P(R)$ profiles exhibit a peak at low radii, $0 \leq R \leq 5$ nm, with a constant position of the maximum ($R_M \sim 2$ nm). The growth of its amplitude with concentration reflects the progressive formation of molecular structures with diameter of ~ $2R_M$. In very diluted systems (C = 0.05; 0.1 wt.%), at the radii R ~ 10-60 nm, larger than the diameter of these structures, the $P(R)$ functions demonstrate a broad peak, indicating an attraction of the structures, probably forming amorphous “clouds”.

However, for the increased concentration (at the critical level C * = 0.2 wt.%) the function $P(R)$ is negative or near zero in the interval $6 < R \leq 60$ nm, characteristic for the repulsion of structures. Similar excluded volume effects, $P(R) < 0$ exist at higher concentrations C = 0.5-1.0 wt.% in a narrow range, R ~ 5-15 nm. At longer distances ($R \sim$ 20-60 nm), the functions $P(R)$ are positive (Fig.S3), a plateau corresponding to structures attraction exists.

Further, the $P(R)$ functions were approximated by the model function (4). Opposite to very diluted systems, more concentrated solutions (C = 0.2; 0.5; 1.0 wt.%) demonstrate substantial excluded volume effects (negative amplitudes g_2), i.e. a low probability of primary units localization in the vicinity of a given object (spacing $R \sim L_A$ with dispersion R_{C2}) (Table S3). Moreover, at a critical concentration (C* = 0.2 wt.%) the amplitude of the third term (g_3) is negative also, and a repulsion is intensive even at long distances $R \leq R_{C3}$. However, in more concentrated systems (C = 0.5; 1.0 wt.%) the amplitude g_3 is positive and the attraction of primary objects dominates at $R \leq R_{C3}$.

It should be mentioned that in the diluted $C_{70}(OH)_{30}$ systems (C = 0.05; 0.1%) the objects observed with $R \leq 1$ nm correspond to single macromolecules or associates of few fullerenols. In spherical approximation, the radius of these objects corresponds to single fullerenols, $R_S = (3/4)R_{C1} \approx$ 0.45 nm. Using Eq. (3) an estimate of the number $m_2 \sim$ 1-2 of coordinated particles near a given object within a sphere of radius $R_{C2} \sim 3$ nm was obtained. Ordering at the radii $R \leq R_{C3} \sim 30$ nm is characterized by a number of coordinated primary objects $m_3 \sim 60$ (Fig.S4). Fullerenols grouping at three levels in aquatic environment is inherent to diluted systems, further enrichment alters molecular interactions and correlations qualitatively.

At the critical point (C* = 0.2 % wt.) the hydrophobic interactions become stronger, stimulating molecules forming the compact groups with correlation radius $R_{C1} \sim 0.9$ nm and diameter $(4/3)2R_{C1} \sim$ 2.4 nm in spherical approximation. The groups are composed of $m_1 \sim 2$ molecules and mutually repell. This is pronounced especially at the distances $R \sim L_A \sim 11$ nm (Table S3, Fig.S4) with effect decreasing at longer distances (Fig.7b). As a result, at C* the system can be considered as a solution of repelling molecular pairs. In more concentrated systems (C > 0.2%), the size of primary objects $R_{C1} \sim 0.9$ nm and the aggregation degree $m_1 \sim 2$ are preserved, but their repulsion weakens and the size of excluded

volume is reduced, $L_A \sim 9$ nm. Attraction between the objects exists at a large scale $R \sim R_{C3} \sim 30$ nm, although the coordination numbers $m_3 \sim 10$ are much lower than in the highly diluted systems. Thus, the ordering of $C_{70}(OH)_{30}$ fullerenols' in dilute solutions, as revealed by SAXS, is basically in agreement with the SANS data (Fig. 6b), showing formation of small molecular groups (1.1-1.3 nm), combined into structures with a radius of ~ 4-7 nm correlating at scales of ~ 30 nm.

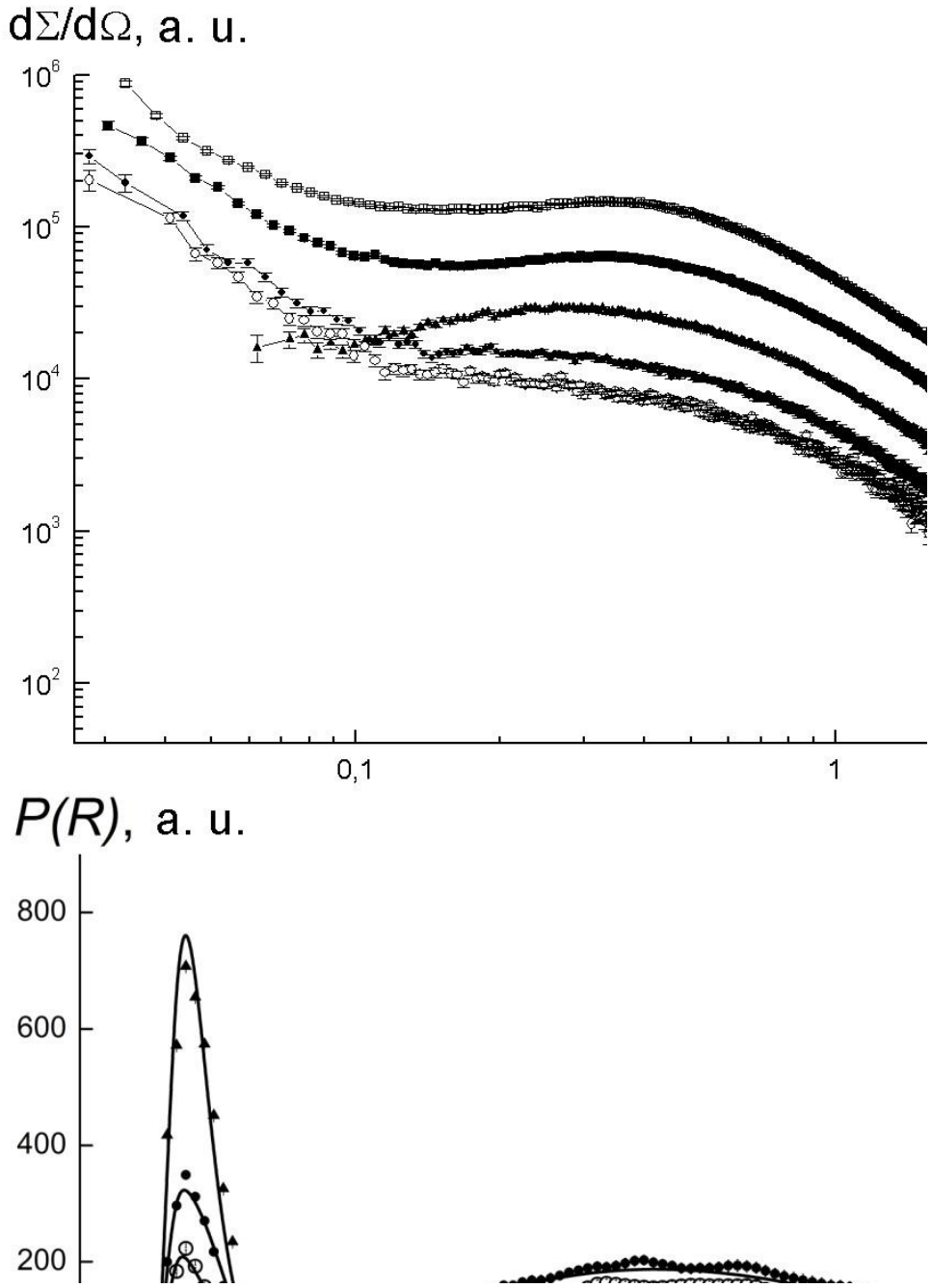

Fig.7. X-ray scattering data for $C_{70}(OH)_{30}$ aqueous solutions: a) concentrations C = 0.05; 0.1; 0.2; 0.5; 1.0 wt. %. (1-5, respectively); b) $P(R)$ functions, concentrations C = 0.05; 0.1; 0.2 wt.%. (1-3), curves correspond to fitting using Eq. (4).

Сделать еще цветом различие

DLS measurements. Complementary/independent/additional? information on $C_{70}(OH)_{30}$ fullerenols assembly in aqueous solutions, was obtained using the DLS experiments on diluted systems (C = 0.1 wt. %) (Fig. 8a). Higher concentrations were not measured because of a high absorption at the laser wavelength, 633 nm. The measurements give more information on fullerenols' ordering in aqueous solutions, especially at submicron scales, inaccessible to small-angle scattering. The obtained hydrodynamic radii of the particles cannot be quantitatively compared with neutron and X-ray data. Still, the light scattering experiments confirm the formation of primary groups of fullerenols as well as the presence of more extended molecular correlations at the distances of >10 nm, and at last, the existence of submicron structures.

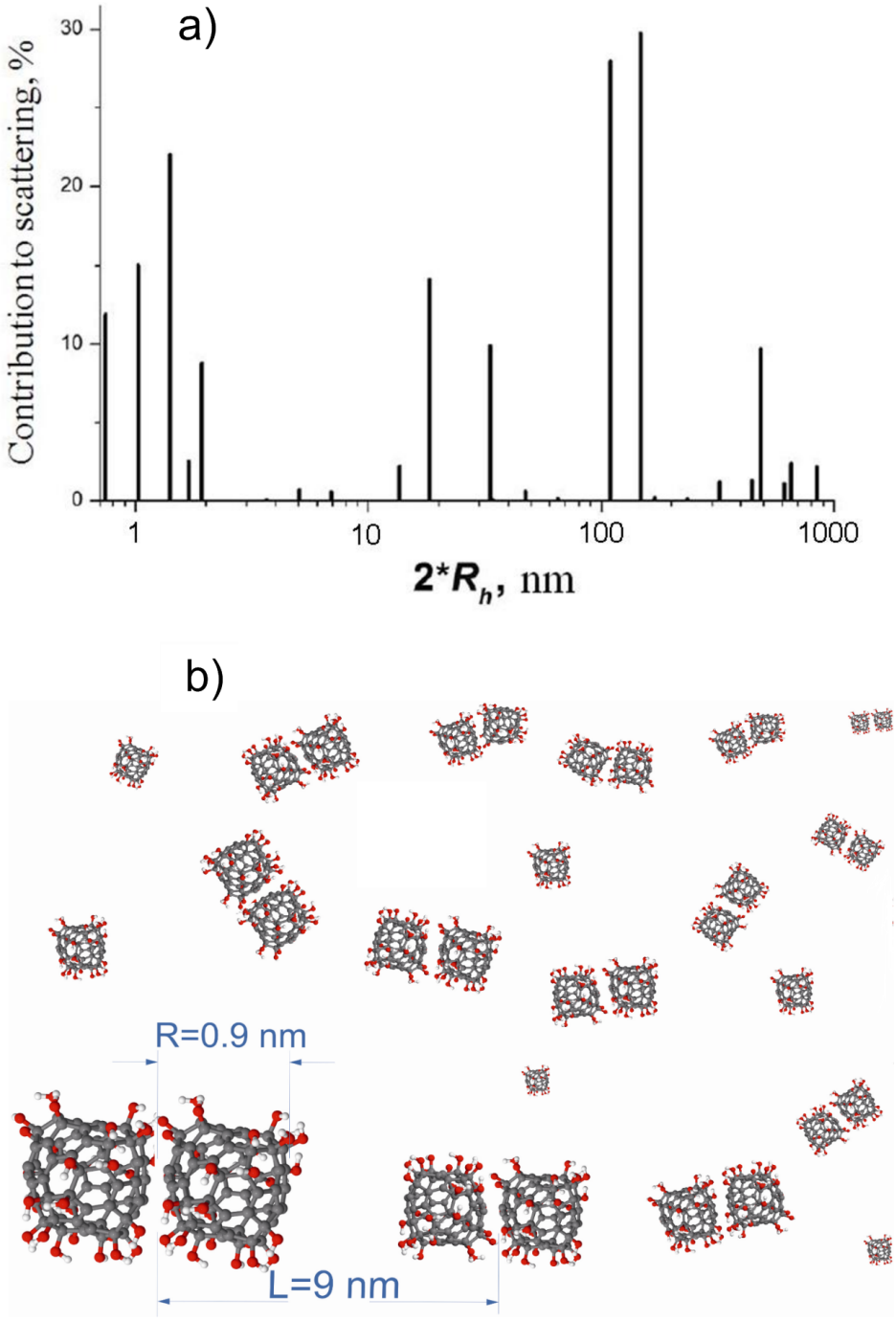

Fig. 8. a) Size distribution of $C_{70}(OH)_{30}$ aggregates in water (pH = 5.6), obtained via DLS in the band of the 16 kHz. b) Schematic representation of self-assembly in the $C_{70}(OH)_{30}$ fullerenols aqueous solutions at the critical concentration C* = 0.2 wt. %. Fig8b – отдельная картинка, или убрать, к ДСР не имеет отношения.

4. Discussion

- Some general words about fullerenols?
- General words on aggregation state on aggregation state of fullerenes, and trends
- Accessible concentration range – an important property?
- Discussion again about multilevel structural organization
- Final words about possible control of aggregation state?
- Perspectives?

Aqueous solutions of fullerenes and their derivatives are a regular object of investigations. The points of interest span from methods of preparation and solubility, to biological properties and toxicity, and also investigations of the cluster state. In this work we report preparation of two types of fullerenols, $C_{60}(OH)_{30}$ and $C_{70}(OH)_{30}$ and structural investigations of their solutions. Such high number of hydroxyl groups was achieved at the second stage of preparation. Characterization of the obtained derivatives via FTIR allowed to reliably estimate the number of OH-groups to be $x=30\pm2$. Hydroxylation indeed varies solubility properties of fullerenes, with the derivatives achieving good solubility in water. A wide range of concentrations of aqueous solutions for produced fullerenols was obtained.

FTIR results were the basis for DFT analysis of the fullerenols structure. The non-uniform covering of the nanoparticles surface by the OH-group seems to be a general feature for different number of hydroxyls, x, in the complex. At high x=30 we obtained the formation of OH-groups chains around the fullerene molecules. The excess hydroxyls form short chains at the molecules "poles". Comparison or discussion of other DFT results?

Small-angle scattering investigations allowed evaluating the structural state of fullerenols in the solutions. The qualitative fits using Eq. (1) were first performed, allowing to evaluate the sizes of agglomerates in the system and their fractal dimensions. Further indirect Fourier transform treatment produces correlation functions for the system, showing specifics of cluster state at different concentrations. Generally, a three-level organization of similar character for $C_{60}(OH)_{30}$ and $C_{70}(OH)_{30}$) is observed. SAXS data was available specifically for $C_{70}(OH)_{30}$ system, yet similar results are expected for the other system. Further, we describe the behavior for $C_{70}(OH)_{30}$ aqueous solution in the whole concentration range of C = 0.05-22 wt.%.

In highly dilute systems ($0.05 \leq C \leq 0.1$ wt. %), separate fullerenols are mostly observed, together with their sparse aggregates (correlation radius ~ 3 nm) joint into large-scale structures (~30 nm). At a specific concentration, C* = 0.2 wt. %, condensation of fullerenols into tiny groups (~ 1 nm in size) is observed. In solution, between the groups repulsion dominates at the distances by an order in magnitude greater their size. Further increase in fullerenols' content up to 1.0% and higher (2-22 wt. %) induces primary groups assembly at the scale R ~ 20-50 nm.

A structural evolution in solutions in the concentration range of C=0.05-1.0 % wt. may be attributed to a consequence of the competition of hydrophobic and electrostatic molecular interactions. As noted above (Fig. S1), in the interval C = 0.05-0.2 wt.% a strong dropping of the hydrogen index (from pH ~ 5 to pH ~ 3) takes place, i.e. the systems acquire pronounced acidic properties by dissociation of fullerenols' hydroxyls. Thus, the increased molecular repulsion induces remarkable

structural changes. In turn, hydrophobic interactions are caused, mainly, by not uniform distribution of OH-groups on fullerenes' surfaces (Fig. 2). Therefore, we may expect that fullerenols in solutions group in a way to contact via their hydrophobic areas. Hence, a formation of chain or branched structures could be probable. The general picture obtained from our investigations is envisaged in the graphical abstract for the article. It should be also noted, that aggregation is a general trend for plain fullerene solutions and their derivatives both in water and other liquid media [34].

Generally, our DLS data are in agreement with previous studies reporting cluster formation with dimensions ~ 1-1000 nm detected by light, X-rays and neutron scattering, optical absorption [13–16] when a type and number of functional groups mostly defined the solubility and aggregation of derivatives of fullerenes and endofullerenes in solutions [18]. However, certain subtle features of functional groups arrangement on the surfaces of fullerenes still are often neglected. Presented quantum-chemical calculations have specified not uniform arrangement of hydroxyls at the surface of carbon cages. Especially, a formation of polar spots of OH-groups and carbon stripes at the equator (Fig.2) stimulates an effective aggregation, which is really observed for fullerenols forced to be glued via hydrophobic surface fragments. A competition of hydrophobic interactions and electrostatic repelling potentials of partially charged fullerenols defines their ordering analyzed above in detail by neutron and X-ray scattering for diluted, moderately and highly concentrated systems. Eventually, peculiar effects of excluded volume were discovered as the factors defining a multi-level ordering of fullerenols.

5. Conclusions

A comparative analysis of the aqueous solutions of $C_{60}(OH)_{30}$ and $C_{70}(OH)_{30}$ by neutron, X-ray and light scattering has revealed a common type of multi-level molecular organization for both kinds of fullerenols. A three-level self-assembly at the scales up to 100 nm is a characteristic feature of fullerenols dissolved in water. The extended molecular order is successively formed by small molecular groups (correlation radius ~ 1 nm) integrated into medium aggregates (radius ~ 3-5 nm), which are organized into large structures of ~ 30 nm in size. No crucial difference in their behaviors even in a wide range of concentrations (0.05-22 wt.%), e.g. at transition from very dilute to dense (gel-like) systems, was revealed.

The concentration dependencies of the structural parameters (sizes, aggregation numbers) of these two systems was obtained. It was shown, that at a primary level the size of molecular groups and the aggregation degree vary insignificantly with C, while at the second and third levels the structural parameters increase by an order of magnitude. The molecular coordination inside primary groups, their arrangement within secondary aggregates and, accordingly, aggregates incorporated into large structures was determined for diluted and highly concentrated systems in connection with the results of quantum chemical modeling of hydroxyls distribution on carbon cages.

The obtained results on molecular organization of fullerenols in aqueous media along with fundamental value have a direct practical importance due to the perspectives of biomedical applications of water soluble derivatives of fullerenes.

Acknowledgements

The authors are grateful to Lisovskaya Lyudmila (PNPI) for useful discussions, assistance in providing FTIR and HPLC analyzes as well as experiments on neutron scattering.

References

[1] G. Bogdanovic, A. Djordjevic, Carbon nanomaterials: Biologically active fullerene derivatives, Srp. Arh. Celok. Lek. 144 (2016) 222–231. doi:10.2298/SARH1604222B.

[2] F.-Y. Hsieh, A. V. Zhilenkov, I.I. Voronov, E.A. Khakina, D. V. Mischenko, P.A. Troshin, S. Hsu, Water-Soluble Fullerene Derivatives as Brain Medicine: Surface Chemistry Determines If They Are Neuroprotective and Antitumor, ACS Appl. Mater. Interfaces. 9 (2017) 11482–11492. doi:10.1021/acsami.7b01077.

[3] A. Ikeda, T. Iizuka, N. Maekubo, K. Nobusawa, K. Sugikawa, K. Koumoto, T. Suzuki, T. Nagasaki, M. Akiyama, Water Solubilization of Fullerene Derivatives by β-(1,3-1,6)-<scp>d</scp> -Glucan and Their Photodynamic Activities toward Macrophages, Chem. - An Asian J. 12 (2017) 1069–1074. doi:10.1002/asia.201700182.

[4] A. Ikeda, T. Mae, M. Ueda, K. Sugikawa, H. Shigeto, H. Funabashi, A. Kuroda, M. Akiyama, Improved photodynamic activities of liposome-incorporated [60]fullerene derivatives bearing a polar group, Chem. Commun. 53 (2017) 2966–2969. doi:10.1039/C7CC00302A.

[5] P. Chaudhuri, A. Paraskar, S. Soni, R.A. Mashelkar, S. Sengupta, Fullerenol−Cytotoxic Conjugates for Cancer Chemotherapy, ACS Nano. 3 (2009) 2505–2514. doi:10.1021/nn900318y.

[6] G. Bogdanović, V. Kojić, A. Đorđević, J. Čanadanović-Brunet, M. Vojinović-Miloradov, V.V. Baltić, Modulating activity of fullerol C60(OH)22 on doxorubicin-induced cytotoxicity, Toxicol. Vitr. 18 (2004) 629–637. doi:10.1016/j.tiv.2004.02.010.

[7] V. Jacevic, V. Djordjevic-Milic, V. Dragojevic-Simic, N. Radic, B. Govedarica, S. Dobric, B. Srdjenovic, R. Injac, A. Djordjevic, V. Vasovic, Protective effects of fullerenol C60(OH)24 on doxorubicin-induced hepatotoxicity in rats: Pathohistological study, Toxicol. Lett. 172 (2007) S146. doi:10.1016/j.toxlet.2007.05.378.

[8] T. Çavaş, N. Çinkılıç, Ö. Vatan, D. Yılmaz, Effects of fullerenol nanoparticles on acetamiprid induced cytoxicity and genotoxicity in cultured human lung fibroblasts, Pestic. Biochem. Physiol. 114 (2014) 1–7. doi:10.1016/j.pestbp.2014.07.008.

[9] J. Grebowski, A. Krokosz, A. Konarska, M. Wolszczak, M. Puchala, Rate constants of highly hydroxylated fullerene C60 interacting with hydroxyl radicals and hydrated electrons. Pulse radiolysis study, Radiat. Phys. Chem. 103 (2014) 146–152. doi:10.1016/j.radphyschem.2014.05.057.

[10] K.J. Moor, S.D. Snow, J.-H. Kim, Differential Photoactivity of Aqueous [C 60] and [C 70] Fullerene Aggregates, Environ. Sci. Technol. 49 (2015) 5990–5998. doi:10.1021/acs.est.5b00100.

[11] R. Zouboulaki, E. Psillakis, Fast determination of aqueous fullerene C 60 aggregates by vortex-assisted liquid–liquid microextraction and liquid chromatography-mass spectrometry, Anal. Methods. 8 (2016) 4821–4827. doi:10.1039/C6AY00885B.

[12] N. Aich, L.K. Boateng, I.V. Sabaraya, D. Das, J.R.V. Flora, N.B. Saleh, Aggregation Kinetics of

Higher-Order Fullerene Clusters in Aquatic Systems, Environ. Sci. Technol. 50 (2016) 3562–3571. doi:10.1021/acs.est.5b05447.

[13] S. Nath, H. Pal, A. V Sapre, Effect of solvent polarity on the aggregation of C60, Chem. Phys. Lett. 327 (2000) 143–148. doi:10.1016/S0009-2614(00)00863-0.

[14] T. Rudalevige, A.H. Francis, R. Zand, Spectroscopic Studies of Fullerene Aggregates, J. Phys. Chem. A. 102 (1998) 9797–9802. doi:10.1021/jp9832591.

[15] V.V. Golubkov, B.A. Shakhmatkin, N.A. Charykov, A. B.M., X-Ray small-angle scattering of fullerene C70 solutions in o-xylene, Russ. J. Phys. Chem. A. 75 (2001) 1667–1670.

[16] H.E. Smorenburg, R.M. Crevecoeur, I.M. de Schepper, L.A. de Graaf, Structure and dynamics of C60 molecules in liquid CS2 from neutron scattering, Phys. Rev. E. 52 (1995) 2742–2752. doi:10.1103/PhysRevE.52.2742.

[17] E. Nakamura, H. Isobe, Functionalized Fullerenes in Water. The First 10 Years of Their Chemistry, Biology, and Nanoscience, Acc. Chem. Res. 36 (2003) 807–815. doi:10.1021/ar030027y.

[18] G. Xing, J. Zhang, Y. Zhao, J. Tang, B. Zhang, X. Gao, H. Yuan, L. Qu, W. Cao, Z. Chai, K. Ibrahim, R. Su, Influences of Structural Properties on Stability of Fullerenols, J. Phys. Chem. B. 108 (2004) 11473–11479. doi:10.1021/jp0487962.

[19] V.P. Sedov, A.A. Szhogina, Method for the preparation of water-soluble derivatives of fullerenes, 2558121, 2014.

[20] T.H. Goswami, R. Singh, S. Alam, G.N. Mathur, Thermal analysis: a unique method to estimate the number of substituents in fullerene derivatives, Thermochim. Acta. 419 (2004) 97–104. doi:10.1016/j.tca.2004.02.001.

[21] M.J. Frisch, G.W. Trucks, H.B. Schlegel, G.E. Scuseria, M.A. Robb, J.R. Cheeseman, G. Scalmani, V. Barone, G.A. Petersson, H. Nakatsuji, others, Gaussian 16, Revision A. 03, Gaussian, Inc., Wallingford CT. (2016).

[22] Jmol: an open-source Java viewer for chemical structures in 3D, (n.d.). http://www.jmol.org/.

[23] R. Ditchfield, W.J. Hehre, J.A. Pople, Self-Consistent Molecular-Orbital Methods. IX. An Extended Gaussian-Type Basis for Molecular-Orbital Studies of Organic Molecules, J. Chem. Phys. 54 (1971) 724–728. doi:10.1063/1.1674902.

[24] A.D. Becke, A new mixing of Hartree–Fock and local density-functional theories, J. Chem. Phys. 98 (1993) 1372–1377. doi:10.1063/1.464304.

[25] C. Lee, W. Yang, R.G. Parr, Development of the Colle-Salvetti correlation-energy formula into a functional of the electron density, Phys. Rev. B. 37 (1988) 785–789. doi:10.1103/PhysRevB.37.785.

[26] T.N. Blanton, C.L. Barnes, M. Lelental, Preparation of silver behenate coatings to provide low- to mid-angle diffraction calibration, J. Appl. Crystallogr. 33 (2000) 172–173.

doi:10.1107/S0021889899012388.

[27] D. Franke, A.G. Kikhney, D.I. Svergun, Automated acquisition and analysis of small angle X-ray scattering data, Nucl. Instruments Methods Phys. Res. Sect. A Accel. Spectrometers, Detect. Assoc. Equip. 689 (2012) 52–59. doi:10.1016/j.nima.2012.06.008.

[28] D.I. Svergun, Determination of the regularization parameter in indirect-transform methods using perceptual criteria, J. Appl. Crystallogr. 25 (1992) 495–503. doi:10.1107/S0021889892001663.

[29] V. Lebedev, Y. Kulvelis, A. Kuklin, A. Vul, Neutron Study of Multilevel Structures of Diamond Gels, Condens. Matter. 1 (2016) 10. doi:10.3390/condmat1010010.

[30] G. Cummins, E. Pike, eds., Optical mixing spectroscopy and photon correlation, M: World, 1978.

[31] A.D. Lebedev, Y.N. Levchuk, A.V. Lomakin, V.A. Noskin, Laser correlation spectroscopy in biology (in Russian), Naukova Dumka, Kyiv, 1987.

[32] T.G. Braginskaya, P.D. Dobitchin, M.A. Ivanova, V. V Klyubin, A. V Lomakin, V.A. Noskin, G.E. Shmelev, S.P. Tolpina, Analysis of the Polydispersity by Photon Correlation Spectroscopy. Regularization Procedure, Phys. Scr. 28 (1983) 73–79. doi:10.1088/0031-8949/28/1/009.

[33] O. V. Boltalina, V.Y. Markov, P.A. Troshin, A.D. Darwish, J.M. Street, R. Taylor, C60F20: “Saturnene”, an Extraordinary Squashed Fullerene, Angew. Chemie Int. Ed. 40 (2001) 787–789. doi:10.1002/1521-3773(20010216)40:4<787::AID-ANIE7870>3.0.CO;2-5.

[34] M. V. Avdeev, V.L. Aksenov, T. V. Tropin, Models of cluster formation in solutions of fullerenes, Russ. J. Phys. Chem. A. 84 (2010) 1273–1283. doi:10.1134/S0036024410080017.